J|A|C|S
ARTICLES
Published on Web 10/09/2002

Pyrolysis in the Mesophase: A Chemist's Approach toward Preparing Carbon Nano- and Microparticles

Lileta Gherghel,[†] Christian Kübel,[‡] Günter Lieser,[†] Hans-Joachim Räder,[†] and Klaus Müllen*,[†]

Contribution from the Max Planck Institute for Polymer Research, Ackermannweg 10, 55128 Mainz, Germany, and FEI Company, Achtseweg Noord 5, 5600 MD Eindhoven, The Netherlands

Received March 11, 2002

Abstract: A mild pyrolytic method is proposed for the generation of different carbon micro- and nanoparticles that are either unprecedented or have never been reported under the present experimental conditions. A hexa-alkyl-substituted hexa-*peri*-hexabenzocoronene serves as a graphite-like starting compound that melts into a discotic liquid crystalline phase prior to heat-induced cross-linking and dehydrogenation. An essential feature of the process is that the liquid crystalline order persists even above 400 °C, i.e., during alkyl chain cleavage. The present approach bears a resemblance to carbomesophase formation during graphitization starting from pitch. The pyrolysis products are characterized by matrix-assisted laser desorption/ionization time-of-flight (MALDI-TOF) mass spectrometry, optical microscopy, selected area electron diffraction (SAED), scanning electron microscopy (SEM), and high-resolution transmission electron microscopy (HRTEM).

Introduction

The chemistry of carbon in the past decade has been dominated by the detection of fullerenes[1] and carbon nanoparticles as new carbon allotropes.[2,3] The latter are of interest not only for fundamental studies of mechanical and electric properties[4] but also for a range of practical applications.[5,6] Preparation of carbon nanotubes, carbon onions, and other classes of carbon particles typically requires high temperature or high pressure.[6] In many examples, carbon materials are synthesized by electric-arc discharge techniques using graphite electrodes[3,7] or laser ablation of graphite targets.[8] Chemical routes have also been attempted.[9] It is well-known that in these cases the reactions are chemically complicated and difficult to control. Pyrolytic methods, such as vacuum pyrolysis, catalytic pyrolysis of organic compounds,[8b,10] and catalytic chemical vapor deposition,[11] can also be utilized to generate carbon nanoparticles.

In contrast to the common pyrolytic syntheses of carbon nanomaterials, which usually occur catalytically or implicate drastic conditions, we propose here a simple and effective new route to carbon nano- and microparticles, by pyrolysis of well-defined polycyclic aromatic hydrocarbons (PAHs) under mild conditions. This approach is completely different from gas-phase and solid-state pyrolysis but has similarity to the classical liquid-phase carbonization of organic precursors such as small aromatic molecules, petroleum, or coal-tar pitches.[12−15] Because of its molecular structure (a two-dimensional disklike graphite subunit)

* Corresponding author: e-mail muellen@mpip-mainz.mpg.de.
[†] Max Planck Institute for Polymer Research.
[‡] FEI Company.

(1) (a) Kroto, H. W.; Heath, J. R.; O'Brien, S. C.; Curl, R. F.; Smalley, R. E. *Nature (London)* **1985**, *318*, 162−163. (b) Krätschmer, W.; Lamb, L. D.; Fostiropoulos, K.; Huffman, D. R. *Nature (London)* **1990**, *347*, 354−358. (c) Sugai, T.; Omote, H.; Bandow, S.; Tanaka, N.; Shinohara, H. *J. Chem. Phys.* **2000**, *112*, 6000−6005. (d) Patney, H. K.; Nordlund, C.; Moy, A.; Rose, H.; Young, B.; Wilson, M. A. *Fullerene Sci. Technol.* **1999**, *7* (6), 941−971.
(2) (a) Müller, T. E.; Reid, D. G.; Hsu, W. K.; Hare, J. P.; Kroto, H. W.; Walton, D. R. M. *Carbon* **1997**, *35*(7), 951−966. (b) Sarkar, A.; Kroto, H. W.; Endo, M. *Carbon* **1995**, *33* (1), 51−55. (c) Dresselhaus, M. S.; Dresselhaus, G.; Saito, R. *Carbon* **1995**, *33* (7), 883−891.
(3) (a) Iijima, S. *Nature* **1991**, *354*, 56−58. (b) Ebbeson, T.; Ajayan, P. M. *Nature* **1992**, *358*, 220−222. (c) Ajayan, P. M. *Chem. Rev.* **1999**, *99*, 1787−1799.
(4) Saito, R.; Dresselhaus, G.; Dresselhaus, M. S. *Physical Properties of Carbon Nanotubes*; Imperial College Press: London, 1998.
(5) (a) Wang, Q. H.; Setlur, A. A.; Lauerhaas, J. M.; Dai, J. Y.; Seelig, E. W.; Chang, R. P. H. *Appl. Phys. Lett.* **1998**, *72*, 2912−2913. (b) Kroto, H.; Terrones, H. *Interdiscipl. Sci. Rev.* **2000**, *25* (1), 78−80.
(6) Ebbesen, T. W. *Carbon Nanotubes*; CRC Press: Boca Raton, FL, 1997.
(7) (a) Iijima, S.; Ichhashi, T. *Nature* **1993**, *363*, 603−605. (b) Bethune, D. S.; Kiang, C. H.; Devries, M. S.; Gorman, G.; Savoy, R.; Vazquez, J.; Beyers, R. *Nature* **1993**, *363*, 605−607. (c) Journet, C.; Maser, W. K.; Bernier, P.; Loiseau, A.; Chapelle, M. L.; Lefrant, S.; Deniard, P.; Lee, R.; Fisher, J. E. *Nature* **1997**, *388*, 756−758.
(8) (a) Thess, A.; Lee, R.; Nikolaev, P.; Dai, H. J.; Petit, P.; Robert, J.; Xu, C. H.; Lee, Y, H.; Kim, S. G.; Rinzler, A. G.; Colbert, D. T.; Scuseria, G. E.; Tomanek, D.; Fischer, J. E.; Smalley, R. E. *Science* **1996**, *273*, 483−487. (b) Guo, T.; Nikolaev, P.; Thess, A.; Colbert, D. T.; Smalley, R. E. *Chem. Phys. Lett.* **1995**, *243*, 49−54.
(9) (a) Faust, R. *Angew. Chem.* **1998**, *37*, 2825−2828. (b) Xie, S.-Y.; Huang, R.-B.; Ding, J.; Yu, L.-J.; Wang, Y.-H.; Zheng, L.-S. *J. Phys. Chem. A* **2000**, *104*, 7161−7164. (c) Lee, C.-Y.; Chiu, H.-T.; Peng, C.-W.; Yen, M.-Y.; Chang, Y.-H.; Liu, C.-S. *Adv. Mater.* **2001**, *13*, 1105−1107.
(10) (a) Endo, M.; Takeuchi, K.; Igarashi, S.; Kobori, K.; Shiraishi, M.; Kroto, H. W. *J. Phys. Chem. Solids* **1993**, *54*, 1841−1848. (b) Diaz, G.; Benaissa, M.; Santiesteban, J. G.; Jose-Yacaman, M. *Fullerene Sci. Technol.* **1998**, *6*(5), 853−866. (c) Jose-Yacaman, M.; Terrones, H.; Rendon, L.; Dominguez, J. M. *Carbon* **1995**, *33* (5), 669−678. (d) Benito, A. M.; Maniette, Y.; Munoz, E.; Martinez, M. T. *Carbon* **1998**, *36* (5−6), 681−683.
(11) (a) Jose-Yacaman, M.; Miki-Yoshida, M.; Rendon, L.; Santiesteban, J. G. *Appl. Phys. Lett.* **1993**, *62*, 657−659. (b) Ivanov, V.; Nagy, J. B.; Lambin, P.; Lucas, A.; Zhang, X. B.; Zhang, X. F.; Bernaerts, D.; Vantendeloo, G.; Amelinckx, S.; Vanlanduyt, J. *Chem. Phys. Lett.* **1994**, *223*, 329−335.
(12) (a) Oberlin, A. *Carbon* **1984**, *22* (6), 521−541. (b) Roche, E. J. *J. Mater. Sci.* **1990**, *25*, 2149−2158.
(13) Oberlin, A.; Bonnamy, S.; Bourrat, X.; Monthioux, M.; Rouzaud, J. N. *ACS Symp. Ser.* **1986**, *303*, 85−98.
(14) Oberlin, A. In *Chemistry and Physics of Carbon*; Thrower, P. A., Ed.; Marcel Dekker Inc.: New York, 1991; Vol. 22.
(15) (a) Marsh, H.; Diez, M. A. In *Liquid Crystalline and Mesomorphic Polymers: Mesophase of Graphitizable Carbons*; Sibaev, V., Lam, L., Eds.; Springer-Verlag: Berlin, 1994; pp 231−257. (b) Hurt, R. H.; Hu, Y. *Carbon* **1999**, *37*, 281−292.

10.1021/ja020363u CCC: $22.00

Chart 1. Molecules **1a** and **1b** and the Concept of the Pyrolytic Approach.

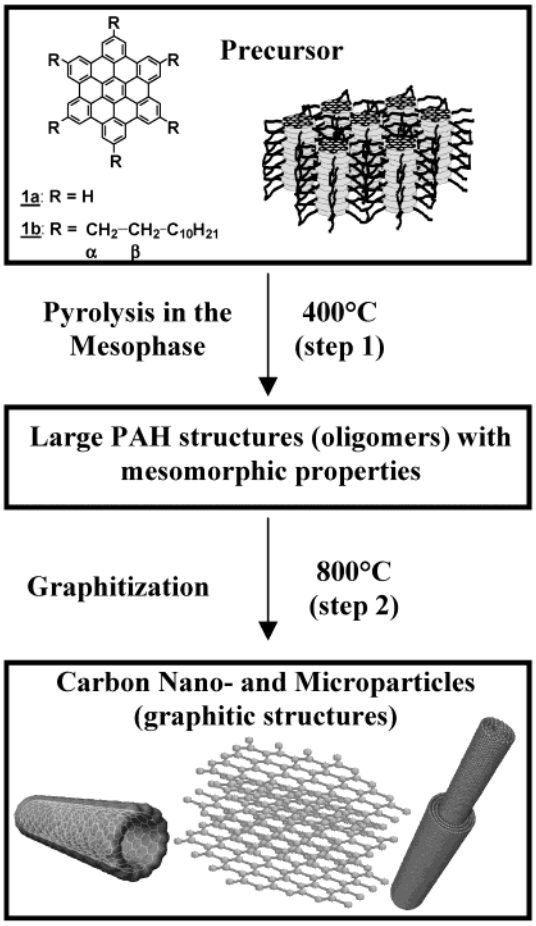

and its exceptional mesomorphic properties, alkyl-substituted hexa-*peri*-hexabenzocoronene (HBC) **1b** (Chart 1) is an excellent candidate for this study.[16] The flexible alkyl chains dramatically lower the melting points and induce the formation of extremely stable discotic mesophases with a columnar arrangement of the disk molecules. This is utilized during thermolysis at moderate temperatures to build up even larger structures that preserve the liquid crystalline (LC) order. The concept rests upon thermal oligomerization of **1b** subunits following the cleavage of alkyl side chains under preservation of the initial mesomorphic order. This enables the lowering of the classical temperature of graphitization and it is expected that, upon further increase of the temperature up to 800 °C, the extended PAH structures would lead to the formation of graphitic structures.

On the basis of this concept, we chose to perform the pyrolysis in two steps: (1) heating to 400 °C to form large intermediate structures and prolonged heat treatment at this temperature to provide a high orientation of these structural units, as a consequence of their mobility in the melt; and (2) further heating to the final temperature at max 800 °C, a temperature remarkably lower than the normally used graphitization temperatures (2000−3000 °C),[12−14] with development of graphite-related structures.

Results and Discussion

A. Formation of Large Mesoscopic Structures. 1. MALDI-TOF Mass Spectrometric Characterization of Products Obtained after the First Step of Pyrolysis. We have recently shown that PAHs such as hexa-*peri*-hexabenzocoronene (HBC) **1a** (Chart 1) and higher homologues can be readily synthesized and characterized as well-defined "graphite" molecules. The synthetic approach, which involves intramolecular cyclodehydrogenation of oligophenylene precursors, can be modified to attach alkyl substituents (**1b**). As mentioned above, alkyl-substituted HBC **1b** shows an extremely stable discotic mesophase and a remarkably wide thermal LC phase window ($T_{k\rightarrow D}$ = 107 °C and max T_i = 417 °C) in which the molecules are organized in an ordered columnar arrangement with a hexagonal superstructure.[16] As previously mentioned, the aim of the first step of the pyrolysis is to obtain a network of PAHs in which the supramolecular order of the liquid crystalline phase is preserved and to stabilize this established order. To elucidate the initial reaction mechanisms and the progress of our "soft-pyrolysis" experiment, the intermediate products were investigated by matrix-assisted laser desorption/ionization time-of-flight mass spectrometry (MALDI-TOF MS) at different time lengths of thermal treatment. Therefore, two pyrolysis experiments were performed with **1b** under identical conditions in evacuated and sealed quartz ampules at 400 °C (for details see Experimental Section). The first ampule was opened after 6 h of thermal treatment and the second after 72 h. The MALDI-TOF measurements were carried out with a sample preparation especially developed for the analysis of commonly insoluble large PAHs. It is known from previous investigations[17,18] that PAHs have to be measured with very soft desorption and ionization conditions because of their tendency to form fragments and coalescence products under laser irradiation. Details of the sample preparation for MALDI-TOF analysis are described in the Experimental Section.

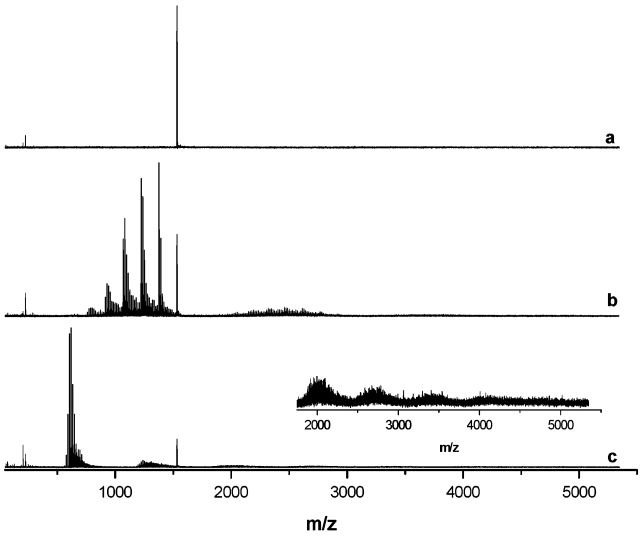

Figure 1. MALDI-TOF mass spectra of pyrolytic products measured with TCNQ as matrix. (a) Starting compound **1b**. (b) Product distribution after 6 h of heating at 400 °C. (c) Product distribution after 72 h of heating at 400 °C; (inset) expanded view of mass range >2000 Da.

The spectrum in Figure 1a was measured before thermal treatment and shows exclusively the molecular ion of **1b** at

(16) Watson, M. D.; Fechtenkötter, A.; Müllen, K. *Chem. Rev.* **2001**, *101*, 1267−1300.
(17) Yoshimura, K.; Przybilla, L.; Ito, S.; Brand, J. D.; Wehmeier, M.; Räder, H. J.; Müllen K. *Macromol. Chem. Phys.* **2001**, *202*, 215−222.
(18) Przybilla, L.; Brand, J. D.; Yoshimura, K.; Räder, H. J.; Müllen, K. *Anal. Chem.* **2000**, *72*, 4591−4597.

1531.3 Da as a radical cation produced by photoionization. The small signals in the low molecular weight region are due to the tetracyanoquinodimethane (TCNQ) matrix. Figure 1b reveals the spectrum of the same sample after heat treatment for 6 h at 400 °C.[19] At this early state of thermal decomposition, numerous new compounds are already visible, which form two main groups of mass distributions around approximately 1200 and 2400 Da. In the lower mass range, near the molecular ion of the intact PAH at 1531.3 Da, a series of intense signals appears with masses of 1377.1, 1222.9, 1068.7, and 914.6 Da. The mass differences are multiples of 154.2 Da and originate from a preferential loss of several $C_{11}H_{22}$ moieties.

Obviously the thermal fragmentation of the complete dodecyl side chains seems to be unfavorable because of the special stabilization of the benzyl-like structures that can be formed when a residual methylene group is left at the HBC core. Mass differences of 14 Da, appearing among the most intense thermal fragments, can be assigned to different numbers of residual methylene units at the HBC core and indicate that the cleavage of the alkyl side groups of **1b** also takes place at any position of the saturated hydrocarbon chain. The second distribution of signals in a mass range between 2000 and 2800 Da in Figure 1b shows, on average, twice the molecular weight of the thermal fragments described before. The interpretation of the exact isotopically resolved masses suggests that this mass distribution is due to dimeric molecules with two intact HBC cores, linked by an alkyl spacer. The close relationship between the low molecular weight distribution around 1200 Da and the high molecular weight distribution around 2400 Da proves that the dimeric molecules are created by a statistical recombination of reactive thermal fragments of **1b** during pyrolysis. A magnified view of the mass region above 3000 Da shows a third distribution of signals around 3600 Da, indicating that even trimeric molecules are formed at this early stage of the process.

The mass spectrum obtained after 72 h of heat treatment of **1b** at 400 °C (Figure 1c) still shows a significant signal of the intact starting compound at 1532 Da, while the structured molecular weight distribution of Figure 1b, which originates from a preferential cleavage of $C_{11}H_{22}$ hydrocarbon chains, has disappeared completely. The most intense signals between 550 and 700 Da are equally spaced by 14 Da and are caused by intact HBC cores bearing different numbers of CH_2 units. The lowest mass of this signal series at 564 Da can be assigned to an intact HBC core substituted with three methyl groups. This demonstrates that the cleavage of alkyl chains now also takes place directly at the aromatic system within this period of extended thermal treatment. The second molecular weight distribution around 1250 Da is due to dimeric HBC molecules as already observed in the spectrum of Figure 1b, however, with significantly lower molecular weights due to the increased loss of alkyl chains. The most intense signal of this series at 1238 Da can be assigned exactly to a chemically bound dimer of a thermal HBC fragment with seven CH_2 units at 620 Da, which is the most probable structure in the low mass region. Whereas the signals of the low mass end of the HBC dimer distribution are equally spaced by 14 Da, this signal structure is lost in the high mass end where a continuum of signals can be observed at each nominal mass value. This can be explained by an increased number of double bonds and rearrangement reactions in the alkyl chains. In addition to the molecular weight distributions of monomers and dimers, higher aggregates (up to heptamers) are observed also at this extended time of pyrolysis.[20a]

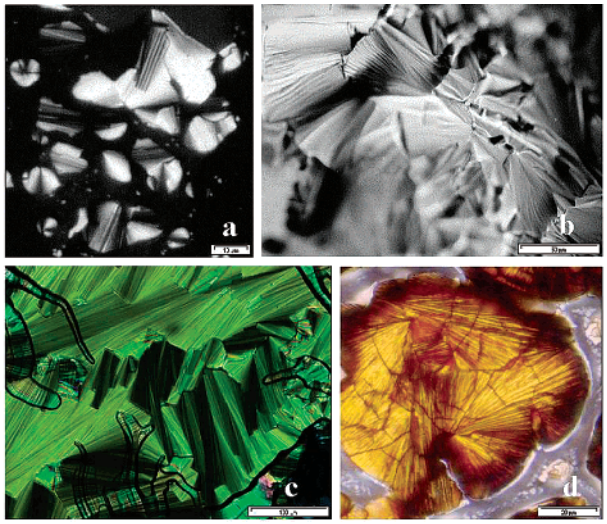

Figure 2. (a) Optical micrograph between crossed polarizers of **1b** after annealing at 400 °C for 72 h; scale bar 10 μm. (b) Surface of the same sample imaged with differential interference contrast in reflected light; scale bar 50 μm. (c) Optical micrograph of **1b** between crossed polarizers after short annealing at 400 °C; scale bar 100 μm. (d) Optical micrograph of **1b** between crossed polarizers after prolonged annealing for 72 h at 400 °C; scale bar 20 μm. The micrographs were recorded at room temperature.

The results of MALDI-TOF mass spectrometry reveal that the oligomerization of **1b** occurs in two steps: (1) preferential cleavage of the C_α–C_β alkyl bonds and formation of free radicals, followed by (2) their intermolecular cross-linking.[20b] The aromatic core of HBC remains intact during heat treatment at 400 °C. With increasing time of pyrolysis, a general tendency toward products with increasing molecular weight and increasing carbon content is observed. From the alteration of the product distribution during the reaction time, it can be concluded that a prolonged pyrolytic decomposition at 400 °C proceeds until the saturated alkyl chains are completely removed or form unsaturated or even aromatic structures themselves by rearrangement or cross-linking reactions.

2. Investigation by Thermogravimetric Analysis and Characterization of Pyrolytic Products (Large Mesoscopic Structures) by Optical Microscopy. Investigation of **1b** by thermogravimetric analysis (TGA), performed under a nitrogen atmosphere at a heating rate of 10 K min^{-1} from room temperature up to 900 °C, shows that the substance is stable up to 300 °C. Above this temperature the decomposition proceeds in two steps. The first step occurs in a temperature range between 300 and 500 °C, showing a weight decrease of 55−58%, and this process can be explained by the gradual loss of alkyl side chains. Above 500 °C the thermal degradation includes the loss of aromatic units. The thermogravimetric analysis of the pyrolytic products of **1b**, obtained by heat treatment for 72 h at 400 °C, was different than that of **1b**. Now the weight loss occurs constantly and completely, in one step, in the temperature range between 450 and 840 °C. Possible

(19) The pyrolytic products obtained by heat treatment for 6 h at 400 °C are soluble in organic solvents and permit the use of conventional techniques for structure elucidation.

(20) (a) Ida, T.; Akada, K.; Okuda, T.; Miyake, M.; Nomura, M. *Carbon* **1995**, *33* (5), 625−631. (b) Lewis, I. C.; Kovac, C. A. *Carbon* **1978**, *16*, 425−429.

Table 1. Overview of the Micro- and Nanoparticles Formed by Mild Pyrolysis

type	description	dimensions	temp (°C)	substrate
A	microspheres (Figure 3a)	diameter a few hundred nanometers to 2 μm	800	quartz
B	microfibers with "bamboo-shaped" structure (Figure 3b,c)	up to 10 μm in cross section and 1−2 mm in length; linear chains of "compartments" of length 10−20 μm	800	quartz
C	nanowires (Figures 3d, 4, and 5)	diameter about 20 nm; lengths from a few hundred nanometers to a few micrometers	800	quartz
D	cylindrical nanorods	outer diameters in the 100 nm range; lengths up to a few micrometers	800	quartz[a]
E	nanorods with 90° kink (Figure 6a)	diameters in the 100 nm range; lengths up to a few micrometers	800	quartz[a]
F	nanoobjects with quadratic geometry[31]	edge lengths a few hundred nanometers to 1 μm	800	quartz[a]
G	nanocolumns (Figure 6b)	square cross sections of about 500 nm, lengths several micrometers	800	quartz[a]
H	doughnutlike nanoparticles (Figure 7)	dimensions less than 200 nm	650	quartz
I	nanosticks (Figure 8a)	100−200 nm diameter and micrometer lengths	650	mica
J	Y-branched nanosticks (Figure 8a)	stems and branches up to 500 nm	650	mica
K	microobjects with hexagonal symmetry and zigzag shape (Figure 8c,d)	1−10 mm cross section and micrometer lengths	650	mica
L	rootlike microobjects[35] (Figure 9)	cross sections 400 nm−1 μm; lengths 30 μm and more	650	mica

[a] Precursor compound **1b** was coated between two quartz plates and preheated at 220 °C.

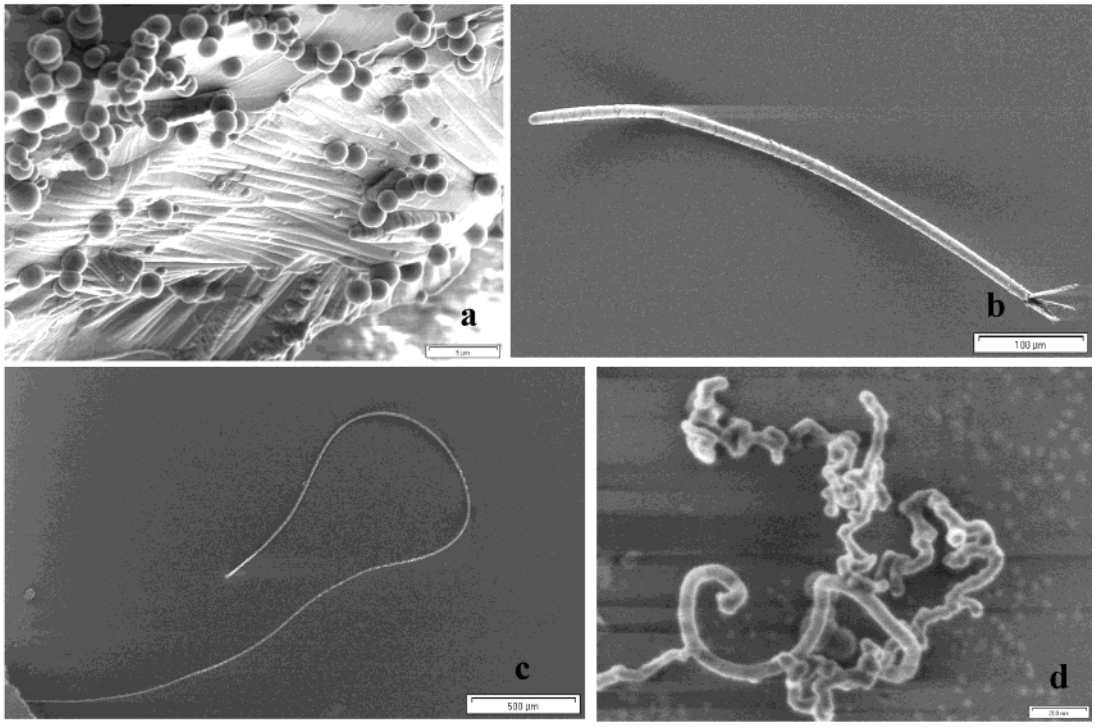

Figure 3. SEM images of micro- and nanoparticles formed by pyrolysis at 800 °C and deposited on quartz. (a) Microobjects with radial spherical texture (type A); scale bar 5 μm. (b, c) Carbon microfibers with bamboo-shaped structure (type B); scale bars (b) 100 μm, (c) 500 μm. (d) Coalescence of the nanowires in the bundle (type C); scale bar 200 nm.

reasons for the finally occurring 100% mass loss of this sample can be either the complete thermal decomposition into volatile fragments or the total oxidation by traces of oxygen.[21]

For a further characterization of the pyrolytic products obtained after heating for 72 h at 400 °C, investigations by optical microscopy between crossed polarizers were conducted. Figure 2a shows well-developed birefringent domains with fanlike textures, which are visible also by differential interference contrast in reflected light (Figure 2b). These textures, typical for a columnar mesophase, suggest that the liquid crystalline order persists even during alkyl chain cleavage and intermolecular cross-linking reactions to form oligomers.

An investigation of the liquid crystalline textures reveals that, above 230 °C, residual areas of the crystalline morphology disappear and domains with fanlike textures emerge, indicating the existence of a columnar discotic phase. These domains grow during heat treatment up to 400 °C. Figure 2c shows the dominant liquid crystalline fanlike texture obtained upon short heating of **1b** at 400 °C. Annealing the sample for 1 h at 400 °C under nitrogen atmosphere does not change the thermal behavior of the sample significantly. Further increase of the temperature leads to the transition into an optically isotropic phase at 420 °C.

Comparatively, the prolonged pyrolysis of the sample for 72 h at 400 °C stabilizes the liquid crystalline texture, and subsequent heating to 600 °C, the maximum temperature attainable with the hot stage of the optical microscope, does not destroy this texture. Figure 2d shows the dominant liquid crystalline fanlike texture upon prolonged annealing of the sample at 400 °C.

(21) For thermogravimetric analysis of **1b** and of the pyrolytic products formed at 400 °C, see Supporting Information.

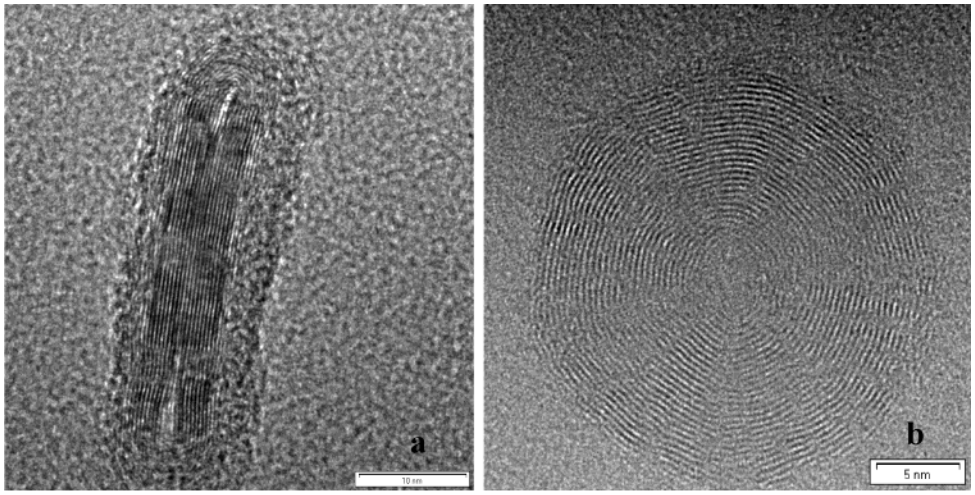

Figure 4. HRTEM images showing isolated graphitic particles; scale bars: (a) 10 nm; (b) 5 nm.

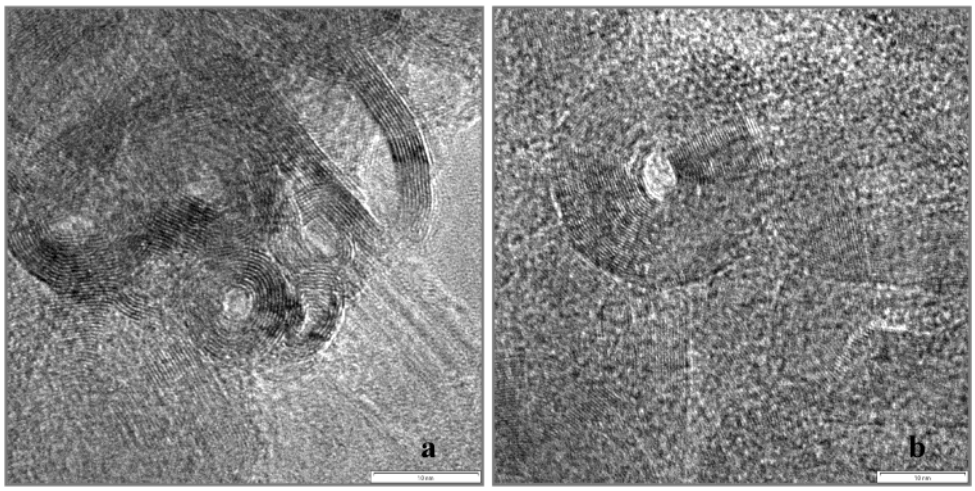

Figure 5. Morphology of the coalescence of the nanowires in the bundle (type C). (a) HRTEM image showing the multiwall stacking of graphite sheets [$d_{(002)} = 3.48$ Å]. (b) HRTEM image showing a hollow circular structure with an unusual bright central core; scale bars: (a, b) 10 nm.

A similar experiment, carried out under prolonged heating for 72 h at only 355 °C, shows that the resulting textures are similar to those in Figure 2d. In contrast to the textures obtained by prolonged heating at 400 °C, they did not resist further heating and transformed at about 425 °C into an isotropic melt. These experiments demonstrate that prolonged heat treatment of **1b** at 400 °C is the best condition for the formation of extremely stable discotic mesophases. Accordingly, **1b** can be pyrolyzed in the mesophase, leading to a network structure in which the mesomorphic order of the pyrolytic products remains preserved. Therefore some preorganization is created before the final pyrolytic step for 24 h at 800 °C.

B. Formation of Graphitic Structures. 1. Effects of Temperature. In the following experiments, the two stages of pyrolysis of **1b** (Chart 1) were carried out successively, without opening of the ampules between the thermal pretreatment at 400 °C and the final pyrolytic step at 800 °C (for details see Experimental Section). Quartz plates were inserted into the ampule as substrate for deposition of pyrolytic products. After completion of the heat treatment, the evacuated and sealed quartz ampules were opened, and the pyrolytic products were collected from the surface of the substrate, as well as from free-standing material in the ampules, and analyzed. The inside walls of the ampules and the quartz plates were coated with a thin (80−100 nm), black film, possessing a metallic luster. Scanning electron microscopy (SEM) examination shows that, in addition, a large quantity of discrete nano- and microobjects were formed (Table 1). The preponderant part of them consisted of free-standing objects in the ampule and the rest of the particles growing on the top of the film, which were unproblematically isolated by mechanical separation. The yield of such structures, estimated by gravimetric determination and by semiquantitative evaluation by optical and electron microscopy, was on the order of 60%. Elemental analysis of the pyrolytic products indicates only a small residual hydrogen content of 0.37−0.42 wt % (original 10.64 wt %).

The structure of the films was analyzed by selected area electron diffraction (SAED), which reveals the characteristic lattice spacing for the 100, 101, 112, and 002 reflections occurring in graphite. The distance between the graphite layers was determined to be 0.348 nm, from the 002 reflection. The diffraction pattern exhibits broad uniform rings indicating graphite grains orientated randomly within the carbon film. However, the 002 reflection forms a sharper diffraction spot with a misorientation of only 35° over an area of 10 μm diameter. Thus the graphite layers oriented perpendicular to the film possess a high long-range order. These results together with the small residual hydrogen content clearly suggest that the films

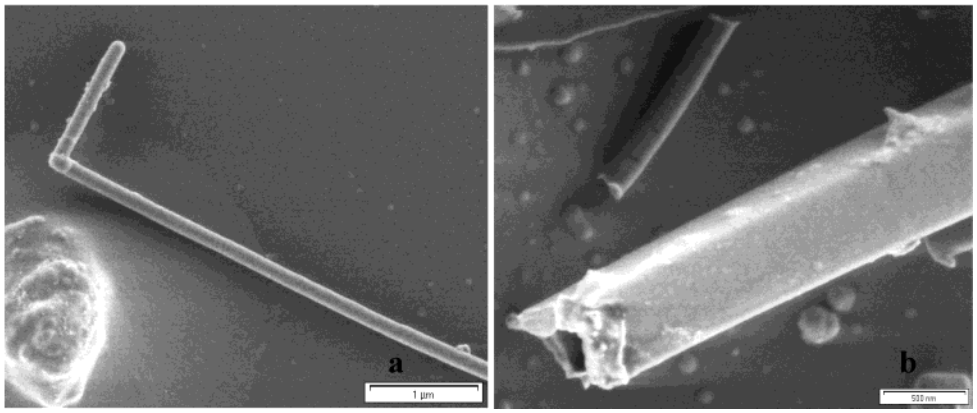

Figure 6. SEM images of polyhedral forms of pyrolytic carbon. (a) Nanorod with kink (type E); scale bar 1 μm. (b) Example of the hollow columns of type G with square cross sections; scale bar 500 nm.

result from the elimination of hydrogen and fusion to larger graphitic structures.

Among the discrete particles were carbon spheres (type A), ranging in diameter from a few hundred nanometers to 2 μm, which at some spots appeared to just emerge from the deposited carbon surface.[12−15,22] The radial spherical textures (Figure 3a) consisted of highly regular single spheres well separated from each other, aggregated spheres, and spherulitic nodules included in the deposited carbon surface. The carbon spheres are comparable to the "mesophase spheres" produced during carbonization of a variety of carbonaceous precursors and reported by Oberlin.[12a] Also present were long carbon microfibers, up to 10 μm in cross section, with a peculiar bamboolike shape (type B). They are composed of linear chains of "compartments", ranging in length from 10 to 20 μm (Figure 3b,c), and resemble CCVD (catalytic chemical vapor deposition) carbon filaments reported by Dresselhaus et al.[23]

The third type of carbon particles detected (type C) were bundles of nanowires, about 20 nm in diameter and ranging in length from a few hundred nanometers to a few micrometers. The SEM image of these coiled nanowires, similar to the filamentous carbon reported by Oberlin[14] upon heat treatment of CO in the presence of metal-based catalysts, is shown in Figure 3d. SAED of type C nanoobjects exhibits the characteristic lattice spacings of graphite powder. A more detailed analysis by high-resolution transmission electron microscopy (HRTEM) shows micrographs that are dominated by graphite layers with a spacing of about 0.348 nm and oriented perpendicular to the electron beam. These graphite layers typically form "multiwall" structures with 5−50 graphite layers[24] and create complex morphologies, consisting of a combination of straight domains, constantly bent walls, closed graphitic band form, and particles with rounded or faceted outer shapes (Figures 4 and 5). The wall thickness and the ratio of straight domains to bent walls vary, giving rise to structural motifs on different length scales.

Remarkably enough, the high-resolution images reveal that many objects consist of aggregates of presumably hollow tubular structures, which exhibit strong contrast, suggesting that they

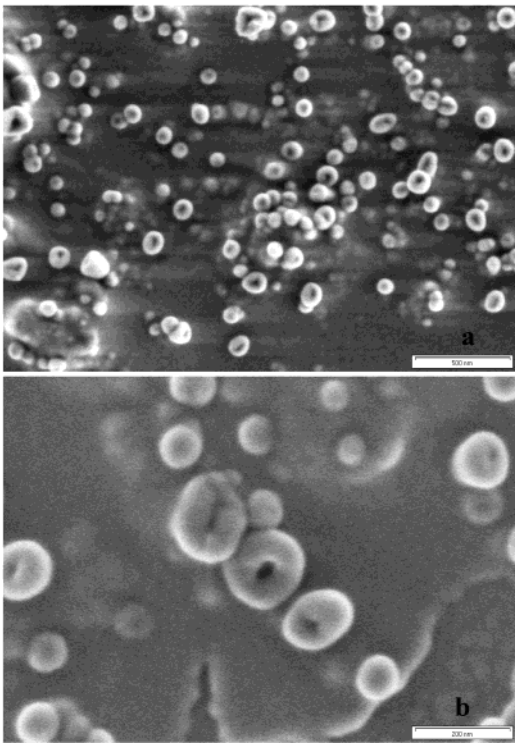

Figure 7. SEM images of round-shaped structures and carbon nanoparticles of type H; scale bars: (a) 500 nm; (b) 200 nm.

are relatively thick in the beam direction (Figure 5). One further notable aspect, clearly illustrated in Figure 5b, is that the central core often appears unusually bright. We therefore suppose that these particles are short tubes. High-resolution images indicate that the tubes have a concentric rather than a spiraling structure and that the central cores of many of these particles are irregular in shape, different from the circular central cores of the classical nanotubes. Another example of a graphitic particle with a remarkable rounded profile, comparable to the spheroidal structure of the type originally reported by Iijima,[25] is shown in Figure 4b. The high-resolution image of this particle exhibits a "multiwall" circular shape with about 25 layers and a regular, uniform contrast (note the disappearance of the empty space in the center).

To study the influence of the temperature profile and simultaneously the importance of the liquid crystalline properties

(22) Hishiyama, Y.; Yoshida, A.; Inagaki, M. *Carbon* **1982**, *20* (1), 79−84.
(23) Dressselhaus, M. S.; Dresselhaus, G.; Sugihara, K.; Spain, I. L.; Goldberg, H. A. *Graphite Fibers and Filaments*; Müller, K. A., Gonser, U., Panish, M. B., Mooradian, A., Sakaki, H., Eds.; Springer-Verlag: Berlin and Heidelberg, 1988.
(24) Ugarte, D. *Carbon* **1995**, *33* (7), 989−993.
(25) Iijima, S. *J. Cryst. Growth* **1980**, *50*, 675−683.

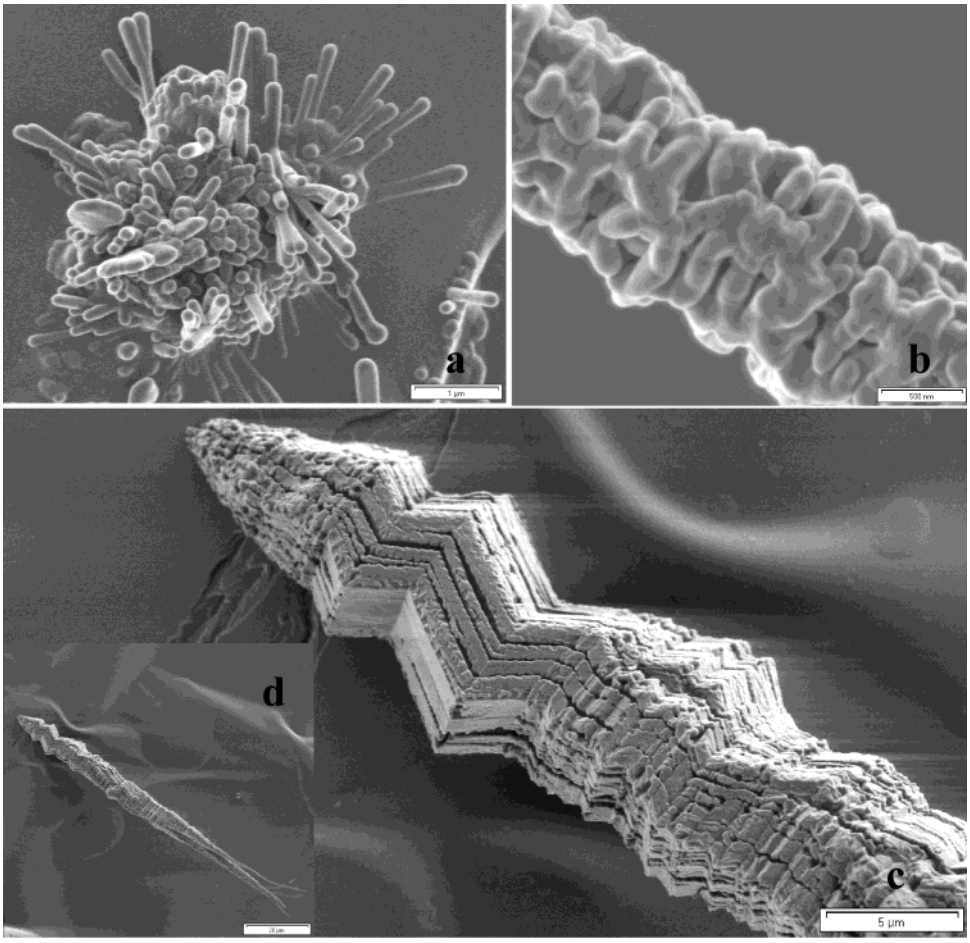

Figure 8. SEM images of carbon pyrolytic structures formed on mica. (a) Carbon nanosticks (type I) and Y-branched carbon fibers (type J); scale bar 1 μm. (b) Fusion of type I and J nanoparticles; scale bar 500 nm. (c) Type K microparticle with hexagonal symmetry and zigzag shape; scale bar 5 μm. (d) Overview of a "giant" (millimeter length) pyrolytic object; scale bar 20 μm.

of **1b** on the formation of pyrolytic products, we applied a second technique for sample preparation: **1b** was coated between two quartz plates and preheated for 10 min to 220 °C, a temperature at which the anisotropic melt was formed but without bond cleavage. After this pretreatment, the quartz plates were inserted into the ampule, which was then evacuated and sealed. The pyrolysis was again conducted in two steps: first for 72 h at 400 °C and then finally for 24 h at 800 °C. SEM studies of the discrete particles formed reveal straight and twisted cylindrical nanorods (type D) as well as nanorods possessing kinks with 90° angles between the arms (type E) (Figure 6a). The columns of type D are round, with thin external walls and large hollow cores, as well as with thick external walls and small hollow cores. The outer diameters lie in the 100 nm range and the lengths are up to a few micrometers. In addition to the particles of type D and E, nanoobjects with a quadratic geometry, like hollow cubes and rectangular parallelepipeds (type F),[26−29] with edges ranging in length from a few hundred nanometers to 1 mm, and micrometer-long columns with square cross sections of about 500 nm (type G) were found (Figure 6b). The latter are new unusual forms of pyrolytic carbon that grow on top of the carbon film perpendicular to its surface.[30] Columns broken off from the base give rise to quadratic craters on the fractured surface.[31] These observations together with the SEM images of the well-defined cages of the broken cubes lead to the conclusion that these objects are hollow. The results of these experiments support the importance of the temperature profile and the final temperature for product formation.

To further examine the influence of the temperature in the final stage of the pyrolysis, several experiments were performed by a similar procedure, with the same temperature profile during the first stage of the pyrolysis (for 72 h at 400 °C) but with differing maximum temperatures during the final stage (see Experimental Section). Thus, when the samples were heated for 24 h at 650 °C, in addition to the bamboo-shaped microfibers (type B), round-shaped, well-separated nanoobjects with small aspect ratio were produced. The latter show often a doughnutlike structure, with a defined channel in the center (type H) (Figure 7).[32]

Alternatively, another experiment was carried out by skipping the thermal pretreatment at 400 °C and heating precursor **1b** directly to 800 °C. As a result, only an irregular film without

(26) Gogotsi, Y. G.; Libera, J. A.; Kalashnikov, N.; Yoshimura, M. *Science* **2000**, *29*, 317−320.
(27) Gogotsi, Y. G.; Yaroshenko, V. P.; Porz, F. *J. Mater. Sci. Lett.* **1992**, *11*, 308−310.
(28) Suzuki, T.; Utsumi, Y.; Sasaki, K.; Shibuki, K. *J. Appl. Phys.* **1995**, *77* (7), 3450−3452.
(29) Saito, Y., Matsumoto, T. *Nature* **1998**, *392*, 237.
(30) Ajayan, P. M.; Nugent, J. M.; Siegel, R. W.; Wei, B.; Kohler-Redlich, P. *Nature* **2000**, *404*, 243.
(31) For SEM images of various forms of pyrolytic carbon formed during the pyrolysis at 800 °C (nanostructures with square cross section), see Supporting Information.
(32) Ihara, S.; Itoh, S. *Carbon* **1995**, *33* (7), 931−939.

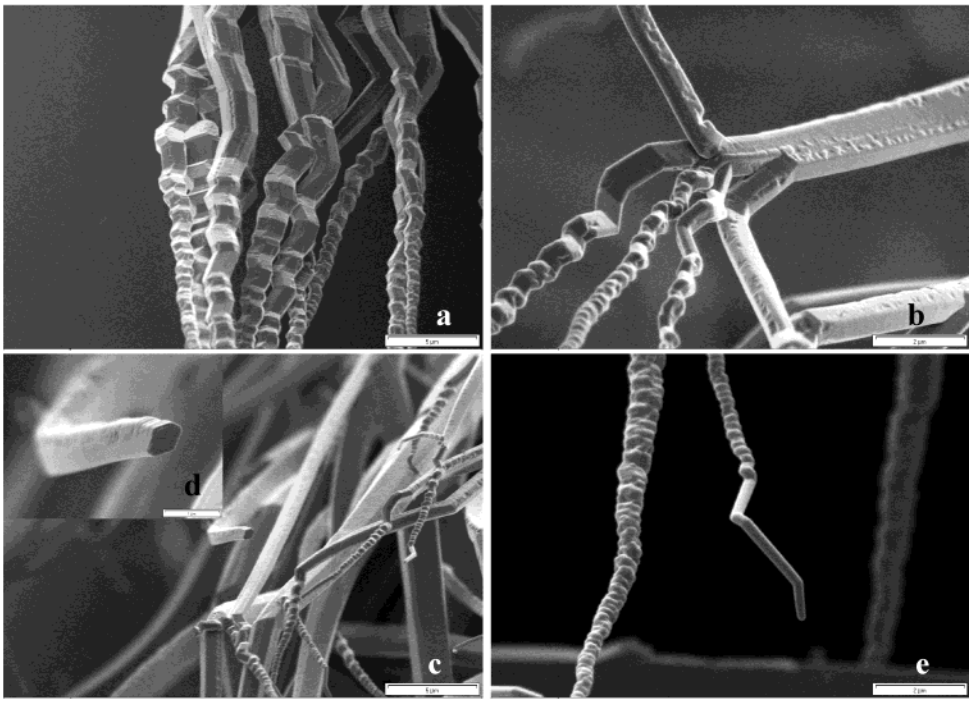

Figure 9. SEM images of microobjects of type L formed by pyrolysis at 650 °C and deposited on mica. (a) Zigzag shape of the branches; scale bar 5 μm. (b) Multiple branched microobject; scale bar 2 μm. (c, inset d) Representative hexagonal cross section of the branches; scale bars (c) 5 μm; (d) 1 μm. (e) Round shape of the top of the branches; scale bar 2 μm.

the presence of micro- and nanoobjects was observed. Since the TGA measurement of sample **1b**, pretreated for 72 h at 400 °C, finally shows a complete decomposition, we cannot exclude completely that the formation of nanoparticles may also take place in the gas phase, possibly by evaporation of reactive fragments. However, the absence of nanoparticles after direct heating to 800 ˚C unambiguously confirms our concept and supports the essential role of the mesophase during the first step of pyrolysis for particle formation.

2. Effects of Substrate. The same procedure and temperature profile during the pyrolysis (heat treatment for 72 h at 400 °C and further heating for 24 h at 650 °C) were utilized for the studies of the role of the substrate on the formation of pyrolytic products. Using mica instead of quartz substrates gave rise to the formation both of films coated on the surface and of discrete particles (Table 1). However, the shape of the latter is significantly different from the ones characteristic for the pyrolytic products deposited on quartz, and the semiquantitative evaluation by optical and electron microscopy of different sites and samples suggests even higher yields of micro- and nanoparticles formed on mica than on quartz. SEM analysis shows that, during the pyrolysis, carbon deposits on mica as a surface with spherulitic morphology and several round nodules emerge from the surface and form nanosticks (type I), with 100−200 nm diameter and micrometer length. Many of them show a three-point junction (type J), similar to the Y-junctions observed by pyrolysis of organometallic precursors or of hydrocarbons with catalysts.[33,34] The SEM image (Figure 8a) indicates Y-branched carbon fibers, consisting of stems and branches up to 500 nm long, and on the top of type I nanoparticles, the initial stage of the formation of Y-junctions. The SEM images in Figure 8b−d suggest the fusion of many nanosticks, at first into structured ensembles, and further to bigger, parallel-oriented structures with hexagonal symmetry and a zigzag shape (type K).

This unusual formation, apparently the preferred structure on mica, was also observed for microobjects of type L (Table 1). These rootlike microobjects,[35] 30 μm and more in length, are filled, multiple-branched, and taper outward to the surface. The branches of the microroots have a hexagonal geometry and cross sections between 400 nm and 1 μm (Figure 9). Only the tops of the branches possess a round shape and in some cases kinks or helical-coiled structures. It must be stressed that these pyrolytic products, with hexagonal symmetry and zigzag shapes, are new and do not correspond to any of the hitherto known types of carbon micro- or nanoparticles.[36, 37]

The growth mechanism of the polyhedral structures of type K and L is clearly different from that observed for the spheres and fibers. We suppose that **1b** or the subsequent pyrolytic products interact with the metal oxides in the mica. This process, which occurs in the interstices between the substrate and the carbon film, supports the formation of nuclei for nanoparticles of type I and J as well as the growth of branched structures and ordered ensembles of the carbon microobjects with hexagonal geometry. It follows that the role of the substrate is decisive for the formation and growth of the pyrolytic products.

3. Role of Alkyl Substitution. The requirement of the liquid crystalline properties of the precursor for our pyrolytic approach is also supported by a further experiment. Unsubstituted HBC **1a**, unable to form an ordered mesophase, was also subjected

(33) Satishkumar, B. C.; Thomas, P. J.; Govindaraj, A.; Rao, C. N. R. *Appl. Phys. Lett.* **2000**, *77*, 2530−2532.
(34) Li, J.; Papadopoulos, C.; Xu, J. *Nature* **1999**, *402*, 253−254.
(35) For SEM image (overview) of a rootlike microobject (type L) formed by pyrolysis at 650 °C and deposited on mica, see Supporting Information.
(36) Endo, M.; Saito, R.; Dresselhaus, M. S.; Dresselhaus, G. *Carbon Nanotubes: Preparation and Properties*; Ebbesen, T. W., Ed.; CRC Press: Boca Raton, FL, 1997; pp 35−110.
(37) Ugarte, D. *Carbon Nanotubes*; Endo, M., Iijima, S., Dresselhaus, M. S., Eds.; Pergamon: Oxford, 1996; pp 163−167.

to pyrolysis, yielding black products completely different from those of **1b**. SEM reveals disordered and spongy structures and the absence of discrete micro- and nanoparticles. These results are fully consistent with literature describing the pyrolysis of unsubstituted PAHs.[38,39] It is obvious that a properly controlled alkyl chain cleavage of **1b** and a "directed" cross-coupling of radical intermediates in an ordered mesophase are key prerequisites for the formation of large mesoscopic structures which further lead to the formation of graphitic structures.

Conclusions and Outlook

We present here a versatile method for producing different forms of carbon micro- and nanoparticles by pyrolysis under soft conditions, in the absence of metal-based catalysts. The extremely stable discotic mesophase of the precursor **1b** provides a preorganization during the first stage of the pyrolysis, which is essential for the pyrolytic "graphitization" in the anisotropic melt. The experiments prove that prolonged heat treatment at 400 °C leads to the formation of large mesomorphic structures by intermolecular coupling reactions and to a stabilization of the mesophase. Further increase of the temperature leads to graphitization processes and the formation of various shapes of carbon nano- and microparticles. Many discrete carbon objects are completely new (types G−I, K, and L) or have never been reported on the present length scale or under the conditions utilized here (types A−F and J).[40−42] Experimental control is possible, e.g., by the substrate and the temperature profile. Some of the nano- and microparticles obtained by our pyrolysis method show many similarities to various flying particles (aerosols) in the atmosphere, which have a significant influence on the regional and global climate and on the formation of clouds.[43] These observations open new perspectives for these pyrolytic products as model systems for certain aerosols. Further studies of the mechanism of selective particle formation are under way, involving especially new PAH starting materials. Our efforts are directed to PAH molecules with ever-increasing π-systems, which are able to form stable discotic mesophases with a stacking of the π-layers. This could lead to designer-made carbon objects for nanoelectronics. An important objective of our further work is also the investigation of the mechanical and electrical properties of these new carbon objects. Micro- and nanomanipulators constitute convenient tools not only for selection of certain particles but also for elucidation of the possibility of reshaping and stretching these particles and for the determination of their electrical conductivity.

Experimental Section

Sample Preparation. All pyrolytic experiments were carried out in evacuated (10^{-5} mbar) and sealed quartz ampules in an electric oven. Typically, the precursor compounds **1a** and **1b** were placed into the ampule together with quartz plates as substrate for deposition of the pyrolytic products and heated at 2 °C/min to 400 °C. This temperature was maintained for 72 h before it was raised for another 24 h to 800 °C or to 650 °C. For the second technique of sample preparation, **1b** was coated between two quartz plates and preheated for 10 min to 220 °C. After this pretreatment, the quartz plates were inserted into the ampule, which was then evacuated and sealed. The samples were then further heated at 400 °C for 72 h and to 800 °C for another 24 h. The pyrolysis products were well reproducible under analogous preparation conditions.

Characterization. For the matrix-assisted laser desorption/ionization time-of-flight mass spectrometry (MALDI-TOF MS) measurements, a sample preparation method was applied that was especially developed for MALDI-TOF analysis of large PAHs.[18] This sample preparation avoids the laser radiation-induced creation of new compounds with lower as well as higher molecular weights than the original molecules, which are only detectable in the mass spectrometer and are not present in the original sample. To make sure that the mass spectra only show the signals of compounds produced by thermal treatment, we applied the matrix 7,7,8,8-tetracyanoquinodimethane (TCNQ) and used only low desorption laser power. Additionally, the samples were prepared by mechanical mixing with the matrix without the use of solvents, which enables also the detection of insoluble compounds possibly produced during thermal treatment.[18,44] The mass spectra were recorded on a Bruker Reflex I MALDI-TOF mass spectrometer equipped with a N_2 laser ($\lambda = 337$ nm) operating at a pulse rate of 3 Hz.

A Zeiss Axiophot optical microscope equipped with polarizers and a nitrogen-flushed Linkam THM 600 hot stage was used to characterize the polarization microscopy textures and to estimate clearing temperatures. Heating and cooling rates varied between 5 and 20 °C min^{-1}.

Elemental analysis were performed at the Institut für Organische Chemie, Johannes Gutenberg-Universität Mainz (Germany).

SAED and SEM investigations were performed on a Leo 912 Omega energy filter transmission electron microscope and LEO 1530 field emission scanning electron microscope, respectively. High-resolution TEM observations were conducted on a CM 20 (200 kV) electron microscope.

Acknowledgment. We thank G. Glasser for the SEM measurements. Financial support by the European Commission (TMR Project SISITOMAS, Project DISCEL and MAC-MES), the European Science Foundation (Project Smarton), and the Bundesministerium für Bildung und Forschung (Multifunctional Materials and Miniaturized Devices Center) is gratefully acknowledged.

Supporting Information Available: Figures showing thermogravimetric analysis of **1b** and of the pyrolytic products formed at 400 °C and SEM images of micro- and nanoparticles of type F and L. This material is available free of charge via the Internet at http://pubs.acs.org

JA020363U

(38) Boenigk, W.; Haenel, M. W.; Zander, M. *Fuel* **1995**, *74*, 305−306.
(39) Fetzer, J. C. *Polycyclic Aromatic Compounds-Very Large PAH Products from Pyrolysis of Mixtures of Smaller PAHs*; OPA: Amsterdam, 1996; Vol. 11, pp 317−324.
(40) Wang, C. Y.; Li, M. W.; Guo, C. T. *Carbon* **1998**, *36* (12), 1749−1754.
(41) Endo, M.; Takeuchi, K.; Kobori, K.; Takahashi, K.; Kroto, H. W.; Sarkar, A. *Carbon* **1995**, *33* (7), 873−881.
(42) Saito, Y. *Carbon* **1995**, *33* (7), 979−988.
(43) (a) Teinemaa, E.; Kirso, U.; Strommen M. R.; Kamens, R. M. *Atmos. Environ.* **2002**, *36* (5), 813−824. (b) G. Helas et al., unpublished studies.
(44) Trimpin, S.; Rouhanipour, A.; Az, R.; Räder, H. J.; Müllen, K. *Rapid Commun. Mass Spectrom.* **2001**, *15*, 1364−1373.